



Analysis of Distortion Mechanism of a Cold Work Tool Steel During Quenching and Deep Cryogenic Treatment

Junwan Li^{1,2} · Yongan Min^{1,2} · Peiyang Wang^{1,2} · Xin Cai^{1,2} · Xiaochun Wu^{1,2}

Received: 17 September 2018 / Accepted: 18 November 2018 / Published online: 30 November 2018
© The Korean Institute of Metals and Materials 2018

Abstract

The microstructure distribution and distortion behavior of a cold work tool steel cylindrical specimen with keyway after quenching (QT) and deep cryogenic treatment (DCT) were evaluated in detail. Furthermore, from the viewpoints of thermal and volumetric strains, an attempt was made to reveal its distortion mechanism during QT and DCT. The results suggest that DCT can effectively improve the dimensional stability of specimen and eliminate the distortion caused by QT. During the QT and DCT processes, the bending direction and the curvature change of specimen are closely associated with the competition between the thermal strain induced by thermal contraction and the volumetric strain caused by martensite transformation. After DCT, the average thermal and volumetric strains of specimen are respectively about -0.0051 mm/mm and 0.0049 mm/mm, which are decreased by about 100% and increased by around 25% compared with that of QT, respectively. During QT, the distortion behavior of specimen is governed primarily by the volumetric strain and it mainly undergoes an expansion deformation. While, during DCT, the distortion behavior of specimen is dominated by the thermal strain and it primarily encounters a contraction deformation. However, compared with the expansion deformation during QT, the contraction deformation of specimen during DCT is much more significant, which further proves that DCT is feasible to improve the dimensional stability of specimen.

Keywords Deep cryogenic treatment · Distortion · Retained austenite · Thermal strain · Volumetric strain

1 Introduction

Distortion is one of the major defects of steel components after heat treatment [1]. Quenching treatment (QT) could lead to unexpected and uncontrolled geometric distortion of the treated parts, and more seriously it may induce cracks in the components [2]. Therefore, it is of great significance to accurately predict and control the heat treatment distortion [3]. In recent years, many researchers have begun to explore the applications of deep cryogenic treatment (DCT), as a supplement to QT, which usually involves cooling the component to -196 °C, holds for several hours and raises

gradually to room temperature [4]. It suggests that DCT is an efficient and useful method to stabilize the internal structure of the metal material [5], enhance the dimensional stability of the steel component [6], and increase the service lifetime of tool [7]. Surberg et al. [8] reported that DCT between the quenching and tempering processes could improve the properties and dimensional stability of AISI D2 steel. Villa et al. [9] indicated that sub-zero treatment can reduce the amount of retained austenite in high-carbon steel and improve its stability. Araghchi et al. [10] designed a novel cryogenic treatment to improve the distortion of a 2024 aluminum alloy. Sonar et al. [11] concluded that, compared with conventional heat treatment, DCT can reduce the distortion potential of AISI D2 tool steel.

However, the influencing factors of distortion are very complicated during heat treatment, especially the occurrence of phase transformation makes it more difficult to control the distortion of components [12]. It is also very difficult to quantitative analysis the distortion behavior of steel component by experimental methods. Fortunately, with the development of numerical simulation, a

✉ Junwan Li
lijunwan@shu.edu.cn

✉ Yongan Min
mya@staff.shu.edu.cn

¹ School of Materials Science and Engineering, Shanghai University, Shanghai 200444, China

² State Key Laboratory of Advanced Special Steel, Shanghai University, Shanghai 200444, China

metallic–thermal–mechanical coupling numerical model for the simulation of quenching has attracted considerable attentions due to its unique advantages [13]. Sugianto et al. [14] adopted the numerical model to research the dimensional changes of components during heat treatment and reveal the origin of quench distortion. It is noteworthy that, at present, the numerical study of DCT focus mainly on the analysis of temperature evolution in component and rarely considers the phase transformation, which cannot accurately depict the distortion behavior occurred in the QT and DCT processes. Therefore, in this investigation, the microstructure distribution and distortion behavior of cylindrical specimen with keyway after QT and DCT were accessed by the direct experimental test. In addition, a metallic–thermal–mechanical coupling finite element simulation using the commercial software DEFORM-HT was performed to reveal the underlying generation mechanism of distortion from the viewpoints of thermal and volumetric strains occurred in the QT and DCT processes.

2 Experimental Procedures

In this work, the cylindrical specimen with keyway was fabricated by a cold work tool steel SDC99 with a chemical composition as follows: 0.91C, 0.51Si, 0.30Mn, 8.60Cr, 1.47Mo, 0.3V, 0.01P, 0.0008S and Fe balance (wt%). Similar to Bok et al. [15], the asymmetric geometry design of cylindrical specimen containing a keyway helps to emphasize the distortion behavior caused by the QT and DCT processes. The geometry and dimensions of the cylindrical specimen with keyway were indicated in Fig. 1. The length (l), diameter (a), height (h) and keyway width (d) of the cylindrical specimen were 100 mm, 10 mm, 7.5 mm and 4 mm, respectively.

For the QT process, the cylindrical specimen with keyway was firstly heated to complete austenitizing and

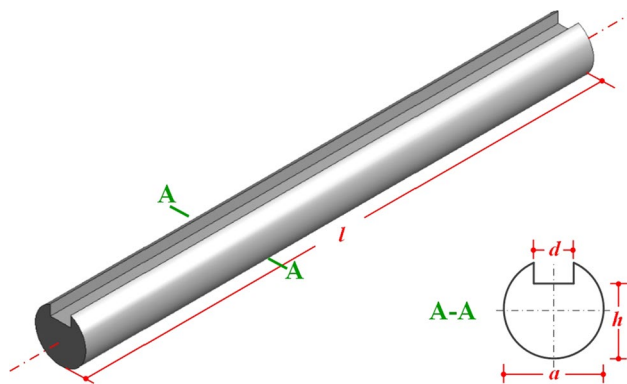


Fig. 1 Geometry and dimensions of cylindrical specimen with keyway

homogenization at 1040 °C for 1 h in a muffle furnace (Nabertherm, LT/24/12/P330, Lilienthal, Germany) under a purified argon atmosphere and then directly cooled by water for 20 min to room temperature. While, for the DCT process, the specimen after QT was immediately placed in a cryogenic tank (SLX-150, Technical Institute of Physics and Chemistry of CAS, China) until its temperature reaches -196 °C. Subsequently, the specimen was taken out of liquid nitrogen and recovered undisturbed at room temperature. After QT and DCT, both the scanning electron microscope (SEM, Zeiss, Supra 40, Germany) and the transmission electron microscope (TEM, JEOL, 2010F, Japan) were used to examine the microstructural characterization of the cylindrical specimen with keyway. The quantitative phase analysis of specimens were carried out by the X-ray diffraction (XRD) instrument (DLMaX-2550, Rigaku, Japan) at room temperature using Cr K α ($\lambda=2.2909$ Å) radiation. The hardness measurement of specimens were performed with a Rockwell hardness tester at a load of 150 kg and duration time of 30 s. The dilatometric test of SDC99 tool steel was conducted using a dilatometer (DIL-805L, BÄHR-Thermoanalyse GmbH, Germany) to estimate the thermal and volumetric strains occurred during heating and cooling. The dimensional changes of cylindrical specimens with keyway after QT and DCT were quantitatively measured by a digital micrometer with a minimum resolution of 0.001 mm.

3 Experimental Result and Analysis

3.1 Microstructure Distribution of Specimen After QT and DCT

Because the SDC99 tool steel belongs to the high carbon and high chrome ledeburite steel with excellent hardenability and hardening capacity, the transformation of austenite to martensite mainly occurs during QT. While, for the DCT process, as claimed in Ref. [16], it mainly involves the phase transformation from the metastable retained austenite contained in specimen to martensite. Furthermore, both Das et al. [17] and Zhirafar et al. [18] proposed that one main purpose of DCT is to eliminate or decrease the retained austenite. Therefore, the evolution and distribution of residual austenite after QT and DCT was mainly taken into account in this study. Figure 2a, b give the measured volume fraction of retained austenite (ξ_A) at different measurement points on the center and bottom of cylindrical specimen with keyway after QT and DCT, respectively. By examining the experimental results presented in Fig. 2, it is found that DCT can significantly decrease the content of retained austenite in the cylindrical specimen. After DCT, both the center and bottom of specimen, the volume fraction of retained austenite (ξ_A) will decrease from almost 15% to about 2%. Meanwhile,

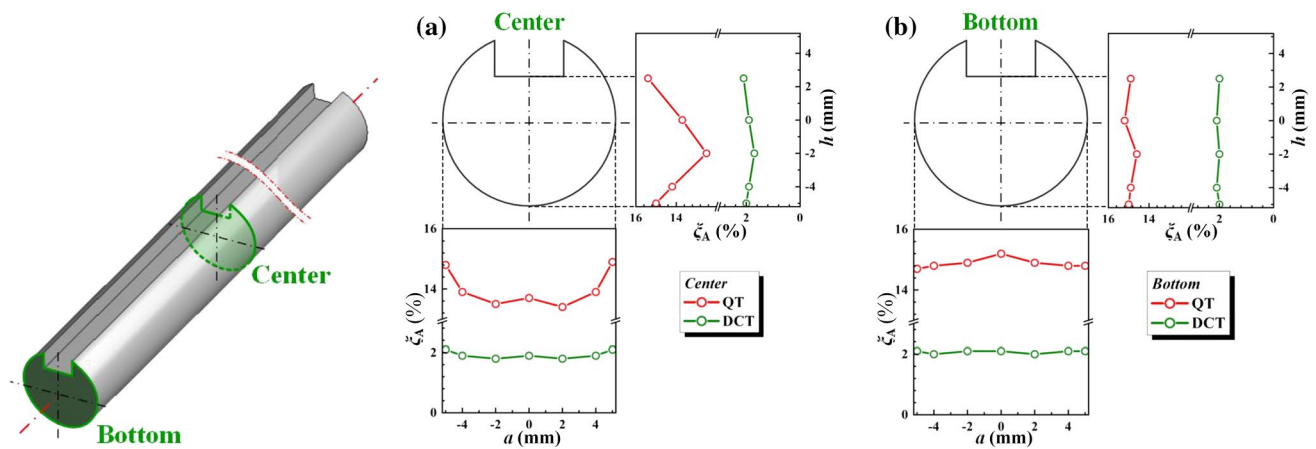


Fig. 2 Volume fraction of retained austenite at different measurement points on the **a** center and **b** bottom of cylindrical specimen with keyway after QT and DCT

the microstructure homogeneity between the center and bottom of specimen after DCT is obviously improved, which is feasible to improve the dimensional stability of specimen. Figure 3 shows the SEM and TEM photomicrographs of cylindrical specimen with keyway after QT and DCT. By comparison of the SEM photographs illustrated in Fig. 3a, c, it is clear that there are more fine and homogeneously distributed of carbide particles precipitated on the matrix of the DCT treated specimen, which is one of the main reasons for the enhancement of mechanical properties (i.e. wear, abrasion and corrosion resistance) of the SDC99 tool

steel after DCT. As claimed in the pioneering works of DCT [19, 20], some hypotheses or speculations suggests that it may be closely related with the driving force for transformation and the thermal activation. However, due to the limitation of experimental conditions, these hypotheses or speculations have not been fully accepted because of the lack of direct evidence. According to the TEM micrographs demonstrated in Fig. 3b, d, there exist some obvious differences in the microstructure morphology between the QT and DCT treated specimens. For the QT treated specimen, it mainly contains martensite and a large amount of metastable

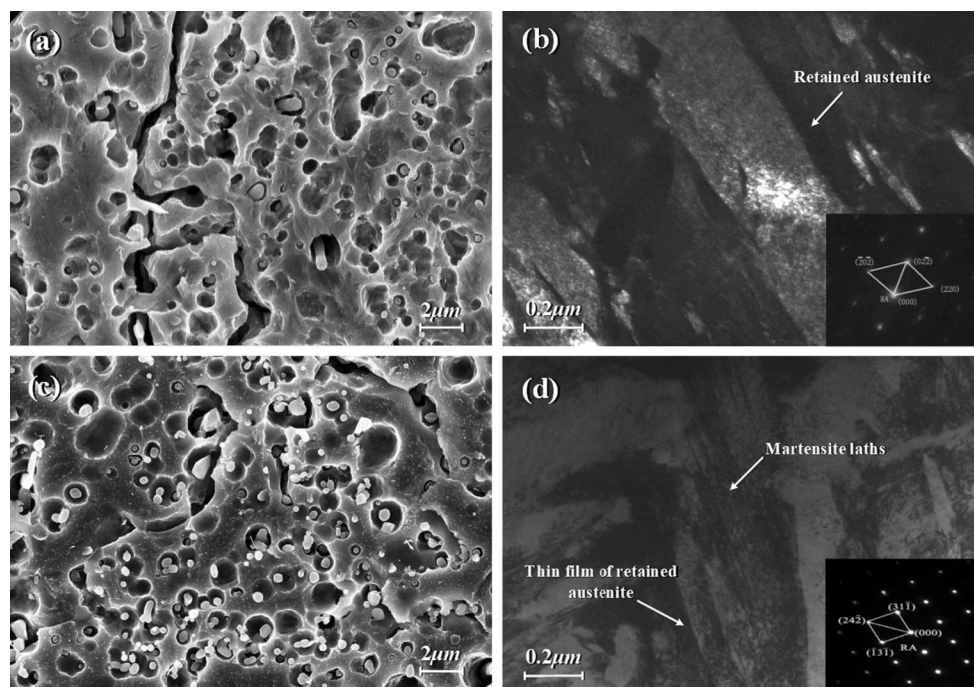


Fig. 3 SEM and TEM photomicrographs of cylindrical specimen with keyway after **a–b** QT and **c–d** DCT

retained austenite, which appears as block or a thick film (> 100 nm). While, for the DCT treated specimen, the matrix is composed of the plate and lath martensite with a high density of dislocation and the thin film of retained austenite (about 10–30 nm). As presented in Fig. 3, during DCT, the metastable retained austenite existed in the QT treated specimen will further transform to martensite and distinctly increase the hardness of specimen. Corresponding to the distribution of retained austenite in the QT and DCT treated specimens presented in Fig. 2, Fig. 4 displays the hardness profile in the center and bottom of cylindrical specimen with keyway after QT and DCT. The Rockwell hardness of the DCT treated specimen achieves approximately 65 HRC. It is significantly higher and more uniform than that of QT, which is closely related to the reduction in the retained austenite content and the improvement of microstructure homogeneity of specimen after DCT.

3.2 Distortion of Specimen After QT and DCT

The elimination or minimization of distortion caused by heat treatments is one of the important issues for improving the quality of steel components. For the purpose of comparison, the cylindrical specimen with keyway is divided into ten 10 mm segments along its longitudinal direction and eleven cross-sections marked with $S_0, S_1, S_2, S_3, S_4, S_5, S_6, S_7, S_8, S_9$ and S_{10} are selected to explore the deformation evolution regularity of specimen during QT and DCT. Figure 5 shows the measured dimensional changes in width and height on the cross-sections of cylindrical specimen with keyway after QT and DCT. According to the measured results, some interesting details can be found: (1) after QT, the dimensional changes in width (Δa) on the cross-sections of cylindrical specimen are noticeably bigger than that in height (Δh). The maximum dimensional changes in

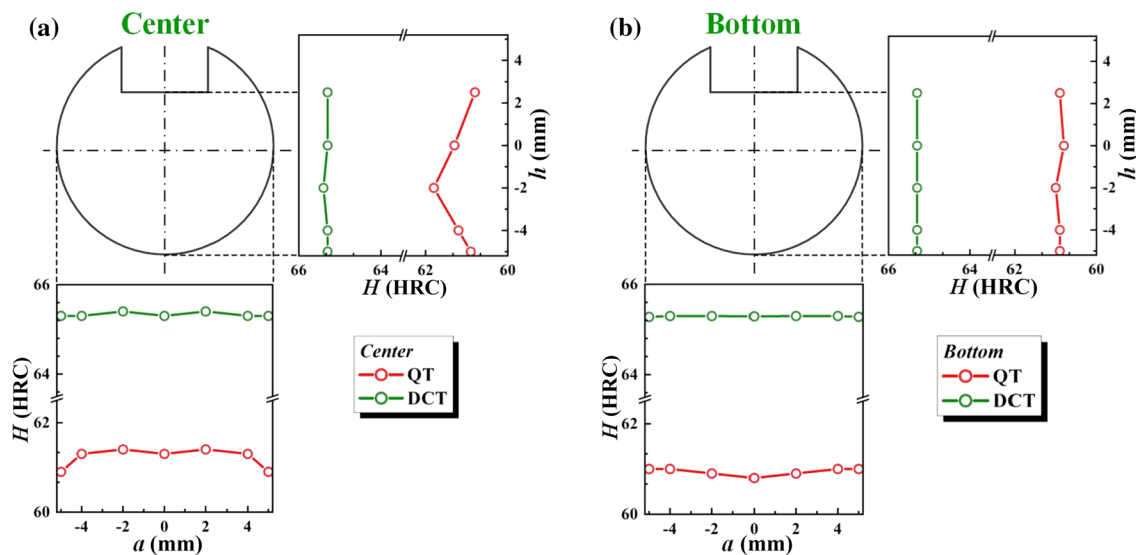


Fig. 4 Hardness at different measurement points on the a center and b bottom of cylindrical specimen with keyway after QT and DCT

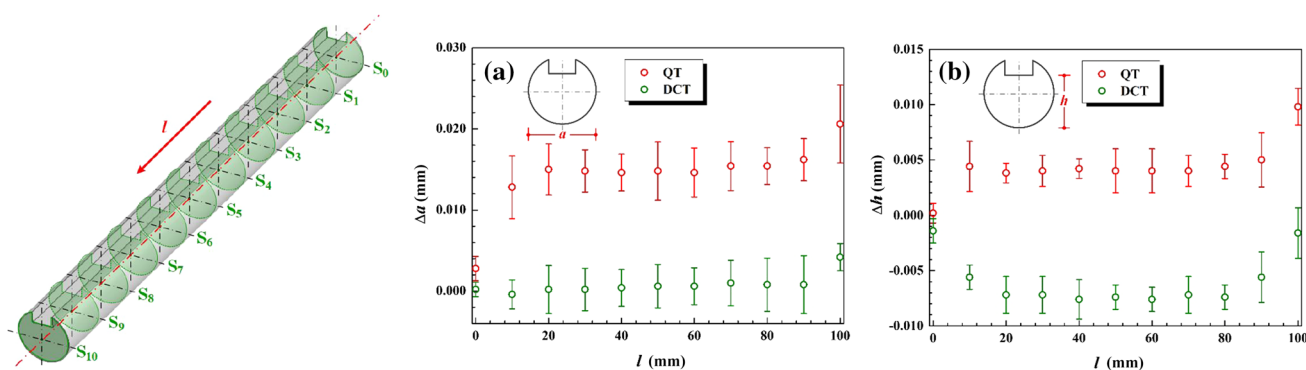


Fig. 5 Measured dimensional changes in a width and b height on the cross-sections of cylindrical specimen with keyway after QT and DCT

width (Δa) and height (Δh) on the cross-sections of cylindrical specimen after QT are approximately 0.0206 mm and 0.0098 mm respectively, which means that there exists a noticeable inconsistency of plastic deformation in the three-dimensional space of specimen during QT and it is not favorable to enhance the dimensional stability of specimen. (2) While, after DCT, both the dimensional changes in width (Δa) and height (Δh) on the cross-sections of cylindrical specimen are decreased significantly, especially that in height (Δh) which even exhibits a state of contraction and its values are negative. The maximum values of dimensional changes in width (Δa) and height (Δh) on the cross-sections of cylindrical specimen have been decreased from almost 0.0206 mm and 0.0098 mm after QT to around 0.0036 mm and -0.0066 mm after DCT, respectively. It indicates that DCT can effectively improve the dimensional stability of specimen and eliminate the distortion caused by QT. Moreover, the measured changes in length of specimen after QT and DCT are 0.206 mm and 0.038 mm, respectively, which presents a similar trend with that in width and height of specimen.

4 Numerical Procedure

4.1 Generation Mechanism of Distortion During QT and DCT

The influencing factors of distortion during QT and DCT are extremely complicated, such as thermal stress, volumetric stress, carbon content and cooling medium, heating and cooling, which makes it very difficult to control in practice. Canale and Totten [21] reported that the generation mechanism of distortion is the non-simultaneity of cooling behavior and phase transformation during heat treatment. Arimoto et al. [22] considered that the origin of quench distortion is closely associated with various types of strains. According to Bok et al. [15], during QT and DCT, the total strain $d\epsilon_{ij}$ increment consists of the elastic $d\epsilon_{ij}^E$, plastic $d\epsilon_{ij}^P$ and thermo-metallurgical $d\epsilon_{ij}^{Tm}$ parts, such that:

$$d\epsilon_{ij} = d\epsilon_{ij}^E + d\epsilon_{ij}^P + d\epsilon_{ij}^{Tm} \quad (1)$$

While, the thermo-metallurgical strain increment $d\epsilon_{ij}^{Tm}$ is decomposed into the thermal $d\epsilon_{ij}^{Th}$, volumetric $d\epsilon_{ij}^{Vol}$ and transformation plasticity $d\epsilon_{ij}^{Trp}$ strain parts as follows

$$d\epsilon_{ij}^{Tm} = d\epsilon_{ij}^{Th} + d\epsilon_{ij}^{Vol} + d\epsilon_{ij}^{Trp} \quad (2)$$

The transformation plasticity strain in this study can be disregarded due to the relatively small size and uniform

cooling condition of specimen during QT and DCT processes. Figure 6 provides a typical strain evolution of SDC99 tool steel in heating and cooling during a dilatometry test. The corresponding thermal and volumetric strains of the tested specimen are presented, respectively. From this figure, it can be observed that the strain is not completely reversible due to the complicated behavior associated with the thermal and phase transformation phenomena and their interactions. Arimoto et al. [22] demonstrated that the origin of quench distortion in specimen can be explained in terms of the thermal and volumetric strains. Therefore, in this investigation, it attempts to reveal the underlying generation mechanism of distortion from the viewpoints of thermal and volumetric strains occurred in the QT and DCT processes.

4.2 FE Model

The numerical simulations considering the coupling of metallurgical, thermal and mechanical phenomena were performed by using DEFORMTM-HT (Scientific Forming Technology Corporation, Columbus, Ohio, USA). The three-dimensional FE model of the cylindrical specimen with keyway prepared for the QT and DCT simulations were demonstrated in Fig. 7. The numbers of nodes and brick elements of specimen were 19,844 and 16,800, respectively. After a fully austenization at 1040 °C for 1 h, the FE model of the cylindrical specimen was assumed to have a homogeneous distribution of temperature and austenite. The physical properties of SDC99 tool steel, especially the low temperature ones, were temperature dependent and the corresponding detail can be found in author's early work [23]. During QT and DCT, the total heat transfer boundary condition considered the convection and radiation were applied on the specimen surface. In author's previous work [24], the heat

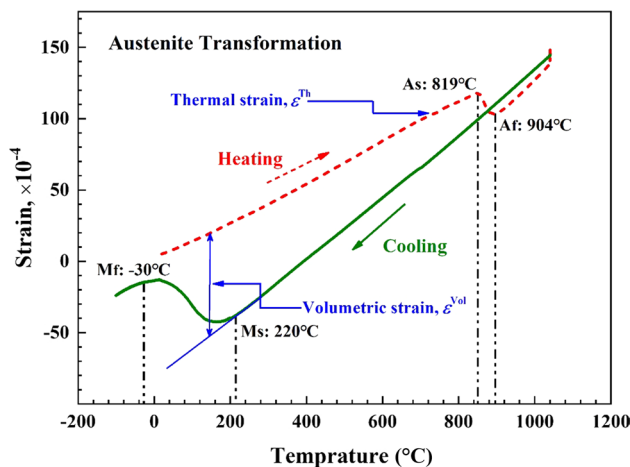


Fig. 6 Thermal and volumetric strains of SDC99 tool steel in heating and cooling during a dilatometry test

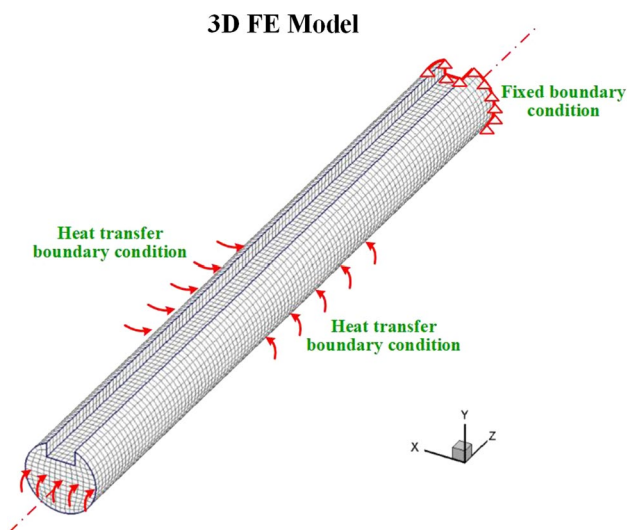


Fig. 7 Three-dimensional FE model of the cylindrical specimen with keyway

transfer coefficients as a function of temperature can also be found. In addition, during the simulations, the fixed boundary condition was applied on the upper end face of specimen, as illustrated in Fig. 7, which means the nodes on the cross-sections S_0 of specimen were fixed in all directions (namely, in the longitudinal, radial and circumferential directions). When all the nodal temperatures of specimen were nearly equal to the temperature of surrounding quenchant, the simulation was terminated.

5 Numerical Result and Analysis

5.1 Verification of FE Model

To verify the prediction accuracy, Fig. 8 illustrates the predicted and measured dimensional changes in width (Δa) and height (Δh) on the cross-sections of cylindrical specimen with keyway after QT and DCT. The predicted dimensional changes after QT and DCT are consistent with the measured data, which indicates that the FE model established in this study can accurately reflect the distortion behavior of cylindrical specimen during heat treatment. Both the predicted and measured results suggest that, compared with QT, DCT can effectively improve the dimensional stability of specimen and eliminate the distortion caused by heat treatment. Moreover, Fig. 9 shows the predicted and measured dimensional changes in length (Δl) of specimen at the end of QT and DCT. Although the predicted dimensional changes in length (Δl) of specimen after QT and DCT (about 0.183 and 0.033 mm) are slightly less than the measured data, they are still well consistent with the measured ones.

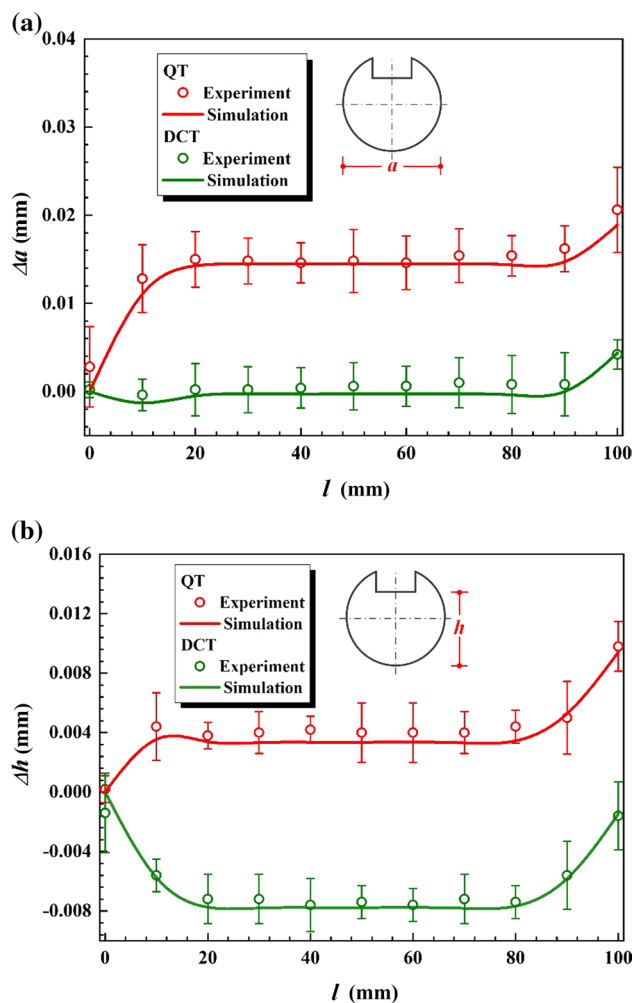


Fig. 8 Predicted and measured dimensional changes in a width and b height on the cross-sections of cylindrical specimen with keyway after QT and DCT

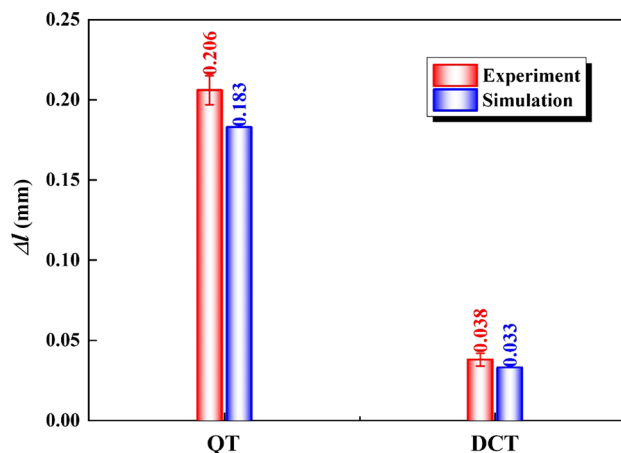


Fig. 9 Predicted and measured dimensional change in length of cylindrical specimen with keyway after QT and DCT

5.2 Thermal Strain

Şimşir and Gür [25] suggests that the thermal strain increment of specimen can be attributed to the thermal expansion coefficient and temperature variation of each phase during heat treatment. For the convenience of explanation, four tracking points (namely, C_1 , C_2 , B_1 and B_2) on the center and bottom cross-sections of cylindrical specimen with keyway are chosen to examine the cooling behavior of specimen during QT and DCT, as demonstrated in Fig. 10. Figure 10a exhibits the time-dependent temperature curves at tracking points C_1 , C_2 , B_1 and B_2 on the center and bottom of specimen during QT and DCT. From the figure, during QT, the temperature variation trends at four different tracking points are similar. However, because the specimen surface is in direct contact with the quenchant, it suffers from intense heat exchange and the temperatures at points C_2 and B_2 present a sharp decrease. On the contrary, the temperature drops at points C_1 and B_1 are relatively slow. While, during DCT, due to the thermal insulation of nitrogen gas at the surface of specimen, it reduces the heat transfer rate and makes the cooling rate of specimen is relatively low. Therefore, the temperature histories of four tracking points during DCT are more slow and gentle than that of QT. Corresponding to the time-dependent temperature curves of four different tracking points C_1 , C_2 , B_1 and B_2 in Fig. 10a, b gives their cooling rate curves in the QT and DCT processes. The cooling rates (V) of four tracking points during QT are significantly faster than that in the DCT process. During QT, the cooling rates on the center and bottom of specimen (namely, C_2 and B_2) reaches their maximum values of about 391 and 555 °C/s at 7.3 and 5.2 s, respectively. While, during DCT, the maximum cooling rates on the center and bottom of specimen are only around 17 and 18 °C/s at 1255 and 1253 s, respectively.

Figure 11 plots the thermal strain (ε^{Th}) evolution at different tracking points on the center and bottom of specimen during QT and DCT. For the QT process, the thermal strain of specimen presents a sharp decline from 0.0165 to

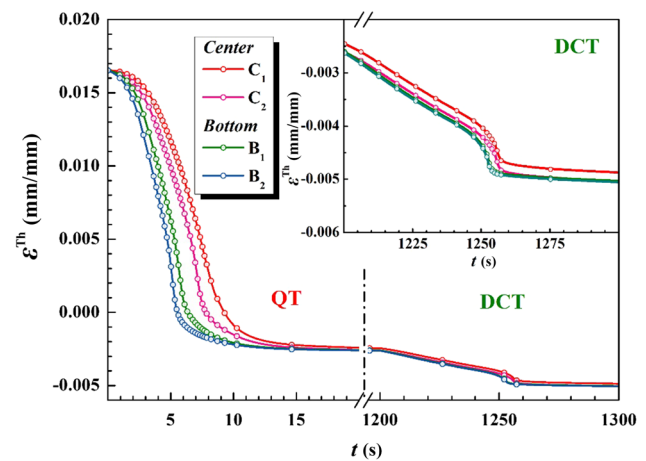


Fig. 11 Thermal strain evolution at different tracking points on the center and bottom of cylindrical specimen with keyway during QT and DCT

–0.0026 mm/mm, especially the tracking points B_1 and B_2 on the bottom of specimen are more obvious. Here, the negative number indicates that the specimen is in a state of thermal contraction and represents a compressive strain. While, for the DCT process, the thermal strain of specimen decreases from –0.0026 to –0.0051 mm/mm. To further explore the spatial distribution and evolution of thermal strain in the specimen during QT and DCT, Fig. 12 displays the predicted spatial distribution of thermal strain in the specimen at different times during QT and DCT. At the initial stage of QT, owing to the rapid cooling of the edge and corner of specimen, it leads to a distinct difference in the cooling rate between the core and surface of specimen, as illustrated in Fig. 10b, which causes an obvious non-simultaneity of cooling behavior and then provokes a non-uniform thermal strain distribution in specimen at 5.96 s of QT. As the cooling time of QT is prolonged, because the cooling rates at the core and surface of specimen tends to be consistent, as displayed in Fig. 10b, the thermal strain of

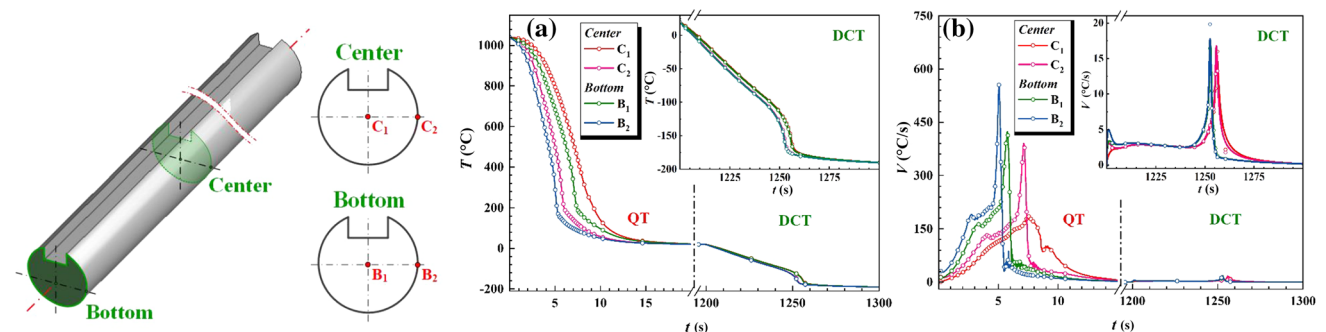
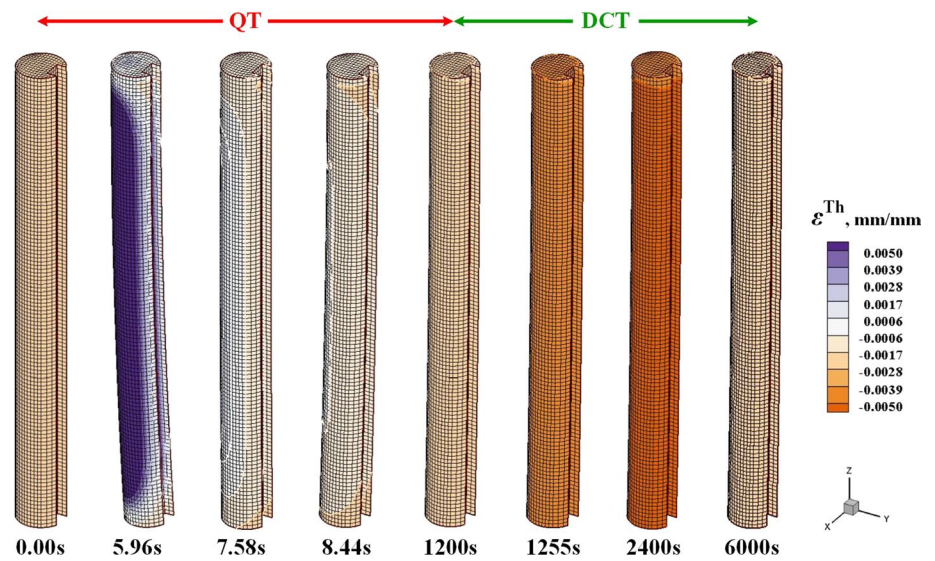


Fig. 10 **a** Temperature and **b** cooling rate curves at different tracking points on the center and bottom of cylindrical specimen with keyway during QT and DCT

Fig. 12 Spatial distribution and evolution of thermal strain in the cylindrical specimen with keyway during QT and DCT



specimen is dramatically decreased and shows a compressive strain. At the end of QT, it represents a uniform distribution and with an average value of about -0.0026 mm/mm. For the DCT process, the thermal strain evolution of specimen exhibits a similar tendency with the QT process. At the end of DCT, the average thermal strain of specimen is approximately -0.0051 mm/mm.

To quantitatively analyze the relationship between thermal strain and dimensional changes, Fig. 13 shows the predicted thermal strain distribution along different tracking lines (namely, l_1, l_2, l_3, l_4, l_5 and l_6) of cylindrical specimen after QT and DCT. The thermal strain distribution along six different tracking lines after QT and DCT have the similar distribution trend in general. After QT, except for the upper end of specimen, the thermal strain of specimen almost shows a uniform distribution and with an average value of compressive strain around -0.0026 mm/mm. The

negative value means the compressive strain. While, after DCT, the thermal strain of specimen continues to decrease from -0.0026 to -0.0051 mm/mm and it nearly doubled after QT. Based on the above analysis, it implies that both the QT and DCT processes will promote the thermal contraction of specimen and this thermal contraction effect is almost the same.

5.3 Volumetric Strain

According to Kamody [26], one of the main purposes of DCT is to continue the phase transformation from the metastable retained austenite contained in components after QT to martensite as much as possible, and to improve the abrasion resistance and dimensional stability of parts. Therefore, to better understand the volumetric strain evolution in specimen during QT and DCT, it is extremely important to

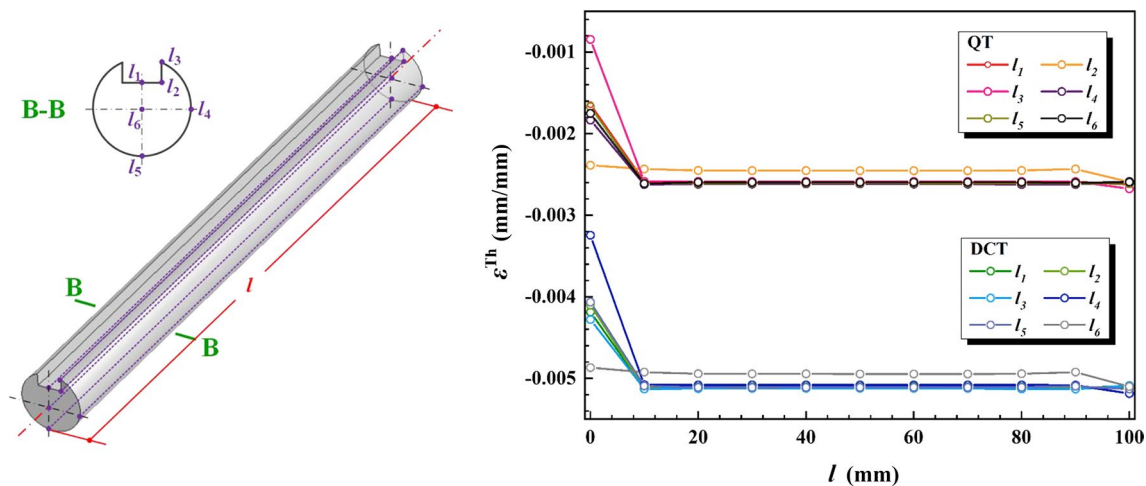


Fig. 13 Predicted thermal strain distribution along different tracking lines of cylindrical specimen with keyway after QT and DCT

firstly evaluate the evolution and distribution of austenite in specimen. Figure 14a, b exhibit the time-dependent volume fractions of austenite (ξ_A) and martensite (ξ_M) at different tracking points C_1 , C_2 , B_1 and B_2 on the center and bottom of cylindrical specimen with keyway during QT and DCT. After QT, the transformation of austenite to martensite is inadequate and about 14.9% of austenite will still be retained in the matrix, as illustrated in Fig. 14a. Subjected to DCT, the amount of the metastable retained austenite contained in specimen is obviously reduced and finally the volume fractions of austenite and martensite in specimen are approximately 2.1% and 97.9%, respectively, as plotted in Fig. 14b. However, it should be stressed that, although the distributions of retained austenite and martensite in specimen after QT and DCT are relatively homogeneous, the non-simultaneity of phase transformation process between the core and surface of specimen is still very evident. It will inevitably lead to the inhomogeneous distribution of volumetric strain in specimen and bring about the distortion of specimen.

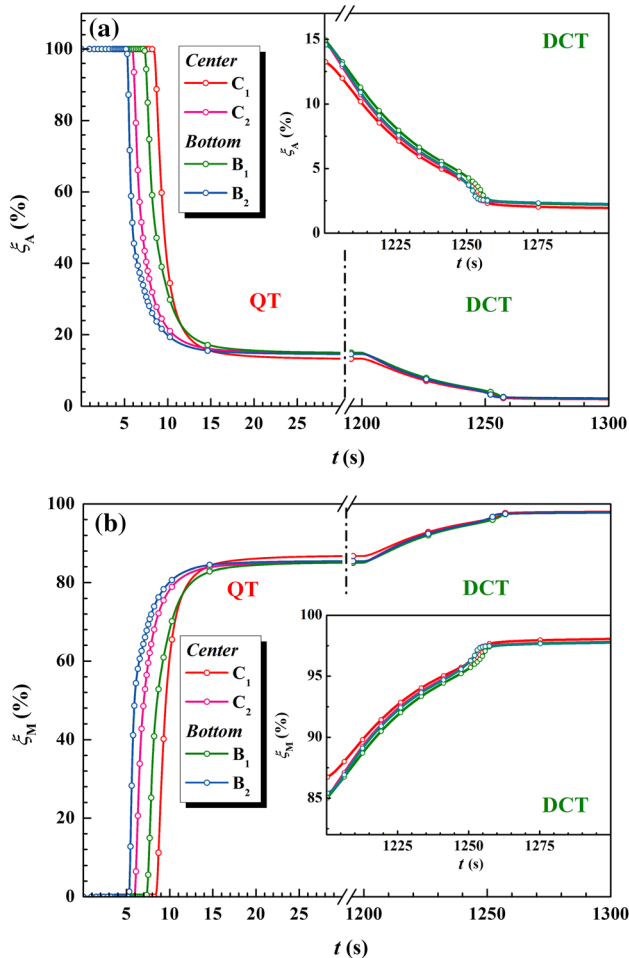


Fig. 14 a Austenite and b martensite evolution at different tracking points on the center and bottom of cylindrical specimen with keyway during QT and DCT

Figure 15 illustrates the volumetric strain (ε^{Vol}) evolution at different tracking points on the center and bottom of specimen during QT and DCT. Correspond to the transformation of austenite to martensite in specimen during QT and DCT, as shown in Fig. 14, the volumetric strain evolution in specimen also shows the similar variation trend and characteristics. According to Fig. 15, in the first 5 s of the QT process, because there is no phase transformation in specimen, the volumetric strain is approximately equal to zero. With the increase of cooling time, due to the asynchronism of phase transformation in specimen, it demonstrates a rapid increase in the volumetric strain of specimen. For the QT process, the volumetric strain of specimen is increased from 0 to 0.0039 mm/mm. Here, the volumetric strain is positive, which means that the specimen is in a state of volumetric expansion and exhibits a tensile strain. While, for the DCT process, because the metastable retained austenite in the QT treated specimen further transforms to martensite, the volumetric strain of specimen will further increase from 0.0039 to 0.0049 mm/mm, which is only increased by about 25% compared with the QT process. Figure 16 gives the spatial distribution and evolution of volumetric strain in the specimen during QT and DCT. The volumetric strain evolution in specimen during QT and DCT is closely related to the transformation of austenite to martensitic. At the initial stage of QT, due to the relatively fast cooling rate at the edge and corner of specimen, its temperature firstly achieves the martensite start temperature (M_s) of SDC99 tool steel (about 220 °C, as shown in Fig. 6). Thus, the phase transformation from austenite to martensitic occurs firstly at the edge and corner of specimen, which makes a remarkable increase of volumetric strain at the two ends of specimen after 5.96 s of QT. Subsequently, with the increase of

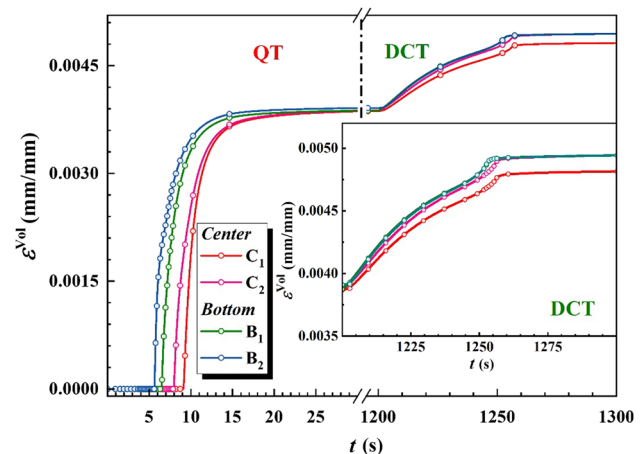
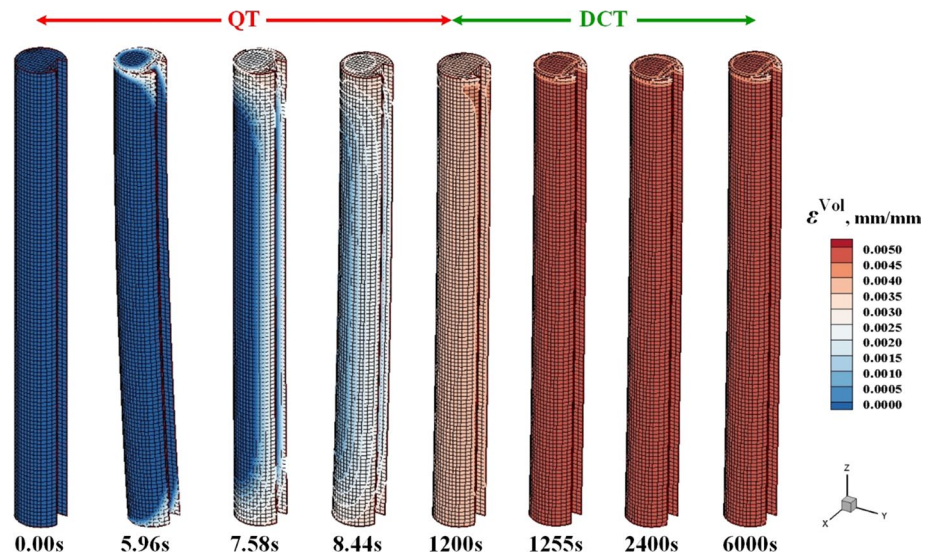


Fig. 15 Volumetric strain evolution at different tracking points on the center and bottom of cylindrical specimen with keyway during QT and DCT

Fig. 16 Spatial distribution and evolution of volumetric strain in the cylindrical specimen with keyway during QT and DCT



cooling time, the volumetric strain in specimen will gradually tend to a uniform distribution. At the end of QT, the average volumetric strain of specimen is about 0.0039 mm/mm. For the DCT process, the change of volumetric strain in specimen is mainly controlled by the transformation of retained austenite to martensitic. At the beginning of DCT, the retained austenite in the QT treated specimen will continue to transform and the volumetric strain in specimen will further increase. After 1255 s of DCT, the temperature of the whole specimen is already below the martensite finish temperature (M_f) of SDC99 tool steel (about $-30\text{ }^\circ\text{C}$, as shown in Fig. 6), most of the retained austenite in specimen has been transformed into martensite and the volumetric strain of specimen shows an evenly distribution. At the end of DCT, the average volumetric strain of specimen is approximately 0.0049 mm/mm. However, it should be pointed out that, due to the volumetric

expansion caused by martensitic transformation, the volumetric strain of specimen both the QT and DCT processes is positive and exhibits a tensile strain.

To investigate the effect of volumetric strain on the distortion behavior, Fig. 17 displays the predicted volumetric strain distribution along different tracking lines $l_1, l_2, l_3, l_4, l_5, l_6$ of specimen after QT and DCT. After QT, apart from the upper end of specimen, the average volumetric strain of specimen is around 0.0039 mm/mm. While, after DCT, the average volumetric strain of specimen will continue to increase from 0.0039 to 0.0049 mm/mm and there is a 25% increase relative to that after QT. By comparing the thermal and volumetric strains distribution along different tracking lines of specimen after QT and DCT illustrated in Figs. 13 and 17, the following information should be mentioned: (1) After QT and DCT, the thermal strain of specimen always presents the compressive strain. While, the volumetric strain

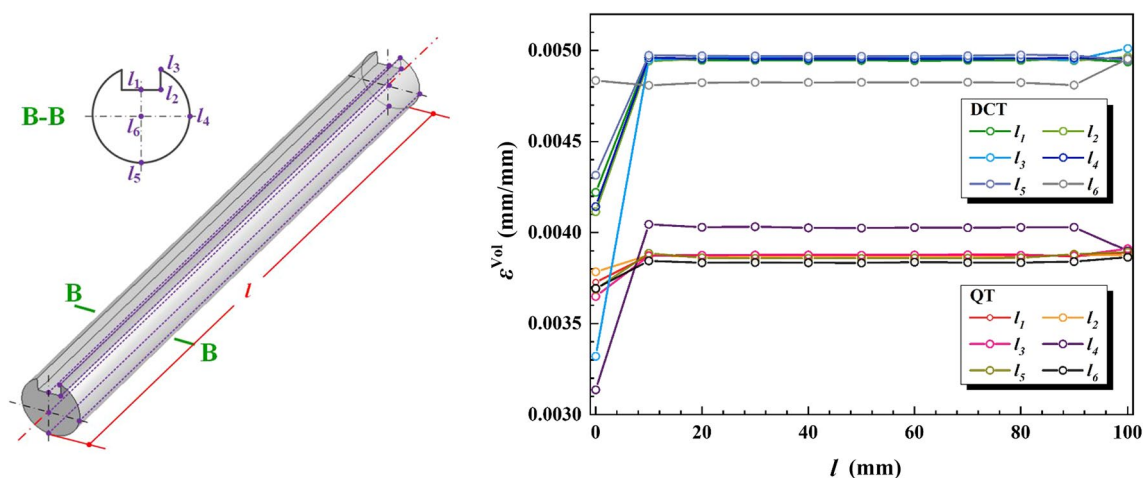


Fig. 17 Predicted volumetric strain distribution along different tracking lines of cylindrical specimen with keyway after QT and DCT

of specimen remains as tensile strain due to the volumetric expansion caused by martensitic transformation. (2) After QT, the average thermal strain (around -0.0026 mm/mm) of specimen is obviously less than its average volumetric strain (about 0.0039 mm/mm), which indicates that the distortion behavior of specimen during QT is governed primarily by the volumetric strain and the specimen mainly undergoes an expansion deformation. (3) Subjected to DCT, the average volumetric strain (approximately 0.0049 mm/mm) of specimen has increased by 0.0010 mm/mm. While, the average thermal strain (nearly -0.0051 mm/mm) of specimen after DCT has decreased by 0.0025 mm/mm, which is almost 2.5 times of its increment of average volumetric strain. It suggests that the distortion behavior of specimen during DCT is dominated by the thermal strain and the specimen primarily encounters a contraction deformation. However, compared with the expansion deformation of specimen during QT, the contraction deformation of specimen during DCT is much more significant, which further proves that DCT is feasible to improve the dimensional stability of specimen.

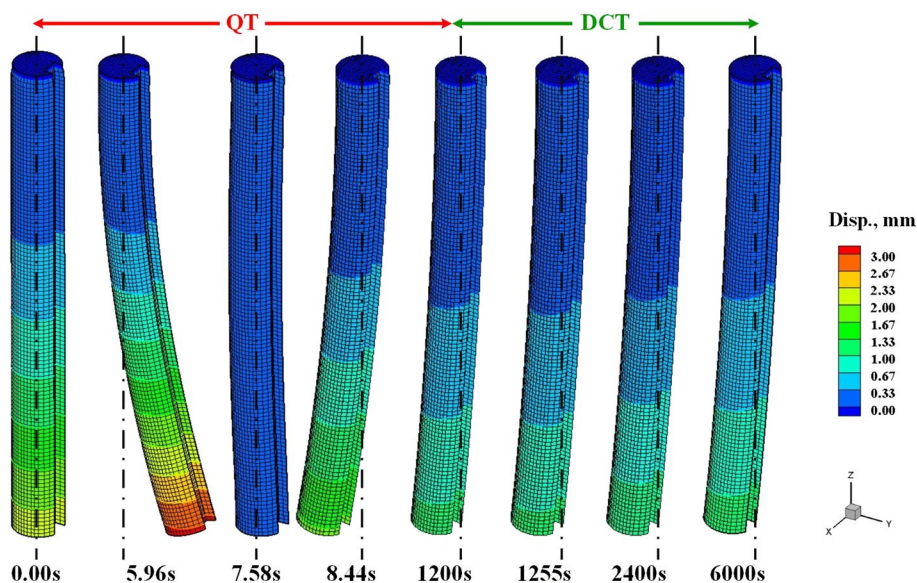
5.4 Dimensional Changes

Figure 18 gives the distortion history (scale factor: $\times 5$) of cylindrical specimen with keyway during QT and DCT. At the beginning of QT, due to the obvious non-simultaneity of cooling behavior between the core and surface of specimen, it will initially lead to the specimen bends toward the keyway side in the normal direction of cutting plane and shrinks along the longitudinal direction of specimen. After approximately 5.96 s of QT, the distortion of specimen reaches a maximum value. Subsequently, with the increase of cooling time, the distortion of specimen tends to be slight at about 7.58 s of QT. After about 8.44 s of QT, because the

temperature of specimen is lower than the martensite start temperature (M_s) of SDC99 tool steel, the transformation of austenite to martensitic occurs and the specimen will begin to bend in the opposite direction. The bending direction of specimen is a result of competition between the thermal and volumetric strains during QT. Based on the foregoing analysis of thermal and volumetric strains during QT, the distortion behavior of specimen during QT in this investigation is governed primarily by the volumetric strain. Therefore, at the end of QT, the specimen will keep its bending direction and undergoes a certain degree of expansion deformation. After entering the DCT process, due to the transformation of metastable retained austenite to martensite, it will cause a volumetric expansion of specimen and reach its peak after about 1255 s of DCT. However, as mentioned previously, the distortion behavior of specimen during DCT is strongly dominated by the thermal contraction strain. Thus, at the end of DCT, the specimen will still keep its bending direction and encounters a contraction deformation.

To further investigate the distortion degree of specimen, because the bending shape of specimen after QT and DCT is consistent with a circular arc, the curvature ($1/r$) is adopted to describe the bending phenomenon of specimen. Figure 19 displays the detail of the curvature change of specimen during QT and DCT. The predicted curvatures after QT and DCT are coincidence well with the measured results, which suggests that the numerical model established in the present study can accurately reproduce the distortion behavior of specimen during QT and DCT. The curvature changes of specimen during QT and DCT represent a “W” shape, which is associated with the competition between the thermal strain induced by the thermal contraction and the volumetric strain caused by the martensite transformation. During QT, the curvature tends to be negative firstly and subsequent appears

Fig. 18 Distortion history of the cylindrical specimen with keyway during QT and DCT (scale factor: $\times 5$)



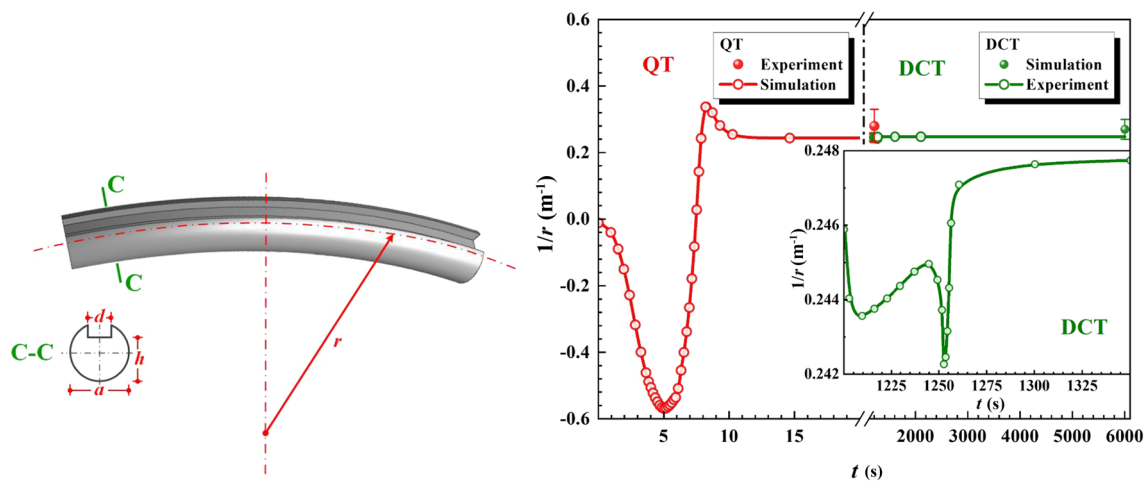


Fig. 19 Curvature changes of the cylindrical specimen with keyway during QT and DCT

to be positive, as plotted in Fig. 19. After QT, the final value of curvature is positive and slightly smaller than the maximum positive value. While, compared with QT, the curvature change of specimen during DCT is always positive and much smaller in its absolute magnitude value, which is attributable primarily to the smaller magnitude of the sum of thermal and volumetric strains occurred at DCT.

6 Conclusion

In this investigation, combining with the metallic–thermal–mechanical coupling FE model, an attempt was made to clarify the underlying distortion mechanism of the cylindrical specimen with keyway during QT and DCT from the viewpoints of thermal and volumetric strains. The major conclusions can be summarized as follows:

- (1) After DCT, the dimensional change of specimen can decrease significantly, especially that in height which even exhibits a state of contraction. It indicates that DCT can effectively improve the dimensional stability of specimen and eliminate the distortion caused by QT.
- (2) At the beginning of QT, owing to the non-simultaneity of cooling behavior, it provokes a non-uniform distribution of thermal strain in specimen. After QT, the specimen represents a uniform distribution of compressive strain and with an average value of about -0.0026 mm/mm. While, after DCT, the average thermal strain of specimen is approximately -0.0051 mm/mm, which is decreased by about 100% compared with QT.
- (3) Due to the asynchronism of phase transformation, it leads to the inhomogeneous distribution of volumetric strain in specimen and brings about the distortion of specimen. After QT, the average volumetric strain of

specimen is about 0.0039 mm/mm and exhibits a tensile strain. While, after DCT, it will further increase to 0.0049 mm/mm because of the phase transformation from retained austenite to martensitic and there is a 25% increase relative to that after QT.

- (4) During QT, the distortion behavior of specimen is governed primarily by the volumetric strain and the specimen mainly undergoes an expansion deformation. While, during DCT, the distortion behavior of specimen is dominated by the thermal strain and it primarily encounters a contraction deformation. However, compared with the expansion deformation during QT, the contraction deformation of specimen during DCT is much more significant, which further proves that DCT is feasible to improve the dimensional stability of specimen.
- (5) During QT and DCT, the cylindrical specimen with keyway will undergo the bending deformation and its curvature change represents a “W” shape. Both the bending direction and the curvature change of specimen are closely associated with the competition between the thermal strain induced by thermal contraction and the volumetric strain caused by martensite transformation.

Acknowledgements This work is supported by the National Key Research and Development Program of China (Grant Nos. 2016YFB0300400 and 2016YFB0300404).

References

1. J.R. Cho, W.J. Kang, M.G. Kim, J.H. Lee, Y.S. Lee, W.B. Bae, J. Mater. Process. Technol. **153–154**, 476–481 (2004)
2. S.J. Lee, Y.K. Lee, Acta Mater. **56**, 1482–1490 (2008)

3. A. Sugianto, M. Narazaki, M. Kogawara, S.Y. Kim, S. Kubota, J. Mater. Eng. Perform. **19**, 194–206 (2010)
4. M. Preciado, P.M. Bravo, J.M. Alegre, J. Mater. Process. Technol. **176**, 41–44 (2006)
5. F.J. Da Silva, S.D. Franco, Á.R. Machado, E.O. Ezugwu, A.M. Souza Jr., Wear **261**, 674–685 (2006)
6. V. Leskovsek, B. Ule, Heat Treat. Met. **29**, 72–76 (2002)
7. H. Li, W. Tong, J. Cui, H. Zhang, L. Chen, L. Zuo, Mater. Sci. Eng. A **662**, 356–362 (2016)
8. C.H. Surberg, P. Stratton, K. Lingenhölle, Cryogenics **48**, 42–47 (2008)
9. M. Villa, K. Pantleon, M.A.J. Somers, Acta Mater. **65**, 383–392 (2014)
10. M. Araghchi, H. Mansouri, R. Vafaei, Y. Guo, Mater. Sci. Eng. A **689**, 48–52 (2017)
11. T. Sonar, S. Lomte, C. Gogte, V. Balasubramanian, Procedia Manuf. **20**, 113–118 (2018)
12. M. Jung, M. Kang, Y.K. Lee, Acta Mater. **60**, 525–536 (2012)
13. D.K. Ju, W.M. Zhang, Y. Zhang, Mater. Sci. Eng. A **438–440**, 246–250 (2006)
14. A. Sugianto, M. Narazaki, M. Kogawara, A. Shirayori, S.Y. Kim, S. Kubota, J. Mater. Process. Technol. **209**, 3597–3609 (2009)
15. H.H. Bok, J.W. Choi, F. Barlat, D.W. Suh, M.G. Lee, Int. J. Plast. **58**, 154–183 (2014)
16. D.N. Collins, Heat Treat. Met. **23**, 40–42 (1996)
17. D. Das, A.K. Dutta, V. Toppo, K.K. Ray, Mater. Manuf. Process. **22**, 474–480 (2007)
18. S. Zhirafar, A. Rezaeian, M. Pugh, J. Mater. Process. Technol. **186**, 298–303 (2007)
19. V.G. Gavriljuk, W. Theisen, V.V. Sirosh, E.V. Polshin, A. Kortmann, G.S. Mogilny, Y.N. Petrov, Y.V. Tarusin, Acta Mater. **61**, 1705–1715 (2013)
20. S.H. Li, M.G. Xiao, G.M. Ye, K.Y. Zhao, M.S. Yang, Mater. Sci. Eng. A **732**, 167–177 (2018)
21. L.C.F. Canale, G.E. Totten, Int. J. Mater. Prod. Technol. **24**, 4–52 (2005)
22. K. Arimoto, S. Yamanaka, M. Narazaki, K. Funatani, Int. J. Microstruct. Mater. Prop. **4**, 168–186 (2009)
23. J.W. Li, L.L. Tang, S.H. Li, X.C. Wu, Mater. Des. **47**, 653–666 (2013)
24. J.W. Li, Y. Feng, H.B. Zhang, N. Min, X.C. Wu, J. Mater. Eng. Perform. **23**, 4237–4250 (2014)
25. C. Şimşir, C.H. Gür, Comput. Mater. Sci. **44**, 588–600 (2008)
26. D.J. Kamody, Adv. Mater. Process. **154**, 215–218 (1998)